A Natural Silk Fibroin Protein-Based Transparent Bio-Memristor

Mrinal K. Hota, Milan K. Bera, Banani Kundu, Subhas C. Kundu,* and Chinmay K. Maiti*

The recent discovery of nanoelectronics memristor devices has opened up a new wave of enthusiasm and optimism in revolutionizing electronic circuit design, marking the beginning of new era for the advancement of neuromorphic, high-density logic and memory applications. Here a highly non-linear dynamic response of a bio-memristor is demonstrated using natural silk cocoon fibroin protein of silkworm, *Bombyx mori*. A film that is transparent across most of the visible spectrum is obtained with the electronic-grade silk fibroin aqueous solution of ca. 2% (wt/v). Bipolar memristive switching is demonstrated; the switching mechanism is confirmed to be the filamentary switching as observed by probing local conduction behavior at nanoscale using scanning tunneling microscopy. The memristive transition is elucidated by a physical model based on the carrier trapping or detrapping in silk fibroin films and this appears to be due to oxidation and reduction procedures, as evidenced from cyclic voltammetry measurements. Hence, silk fibroin protein could be used as a biomaterial for bio-memristor devices for applications in advanced bio-inspired very large scale integration circuit design as well as in biologically inspired synapse links for energy-efficient neuromorphic computing.

1. Introduction

Recent discovery of the memristor (resistor with memory) is predicted to make a massive leap in revolutionizing the design of electronic circuits for a number of applications, such as non-volatile memory to programmable logic. Its attractive features include scalability, low power consumption and dynamic responses.[1–5] The memristor is a fourth fundamental passive circuit element, where resistance varies according to its previous involvement in the signal transfer processes, i.e., it combines the properties of resistance with memory. Mainly, inorganic, polymeric, and organic materials have been found to exhibit memristor properties.[6–12] Recently, the memristive switching characteristics has been demonstrated in ferritin protein; however, the presence of inorganic ions such as iron ions in the form of hydrous ferric oxide [Fe (III) O.OH] is reported to be responsible for resistive switching.[13]

State-of-the-art, the bio-inspired electronic circuit design along with information processor has opened up new vistas for the fabrication of unconventional computing systems, which are able to process information as - brain does. Undoubtedly, the bio or organic devices promise to transform the extent of and access to electronics by providing remarkably inexpensive, light weight and capable ubiquitous components that are printed onto transparent glass or flexible plastic materials.[14] Despite such immense potentiality, the use of electronic circuit in bio-electronic memory is restricted owing to issues with biocompatibility amongst circuit materials. Among a few bio-electronic materials, silk fibroin of silkworms represents a unique family of structural proteins that are biocompatible, biodegradable, mechanically superior, and can be chemically modified to suit a wide range of tissue engineering[15–17] and regenerative medicine,[16] as well as other biomedical applications.[19–26]

Here, a practical strategy of utilization of silk bio-memristor as programmable dynamic load for advance bio-inspired electronic circuit design is employed. An attempt is made to model the physico-chemical mechanisms involved in memristive switching behavior of the bio-memristors based on natural pure silk fibroin protein.

2. Results and Discussion

UV-vis transmission spectrophotometer was used to study the transparency of the device (2% silk fibroin (SF) protein on indium-tin-oxide (ITO) coated glass) as shown in **Figure 1**a. ITO coated glass sample was used for baseline correction. Spectral evaluation showed high transmission (transmittance between 90 and 95%) across most of the visible spectrum, which established the film to be transparent. Amino acid composition of silk

M. K. Hota, M. K. Bera, C. K. Maiti
Department of Electronics and Electrical Communication Engineering
Indian Institute of Technology
Kharagpur 721302, India
E-mail: m.k.bera.iitkgp@gmail.com
B. Kundu, S. C. Kundu
Department of Biotechnology
Indian Institute of Technology
Kharagpur 721302, India
E-mail: kundu@hijli.iitkgp.ernet.in

DOI: 10.1002/adfm.201200073

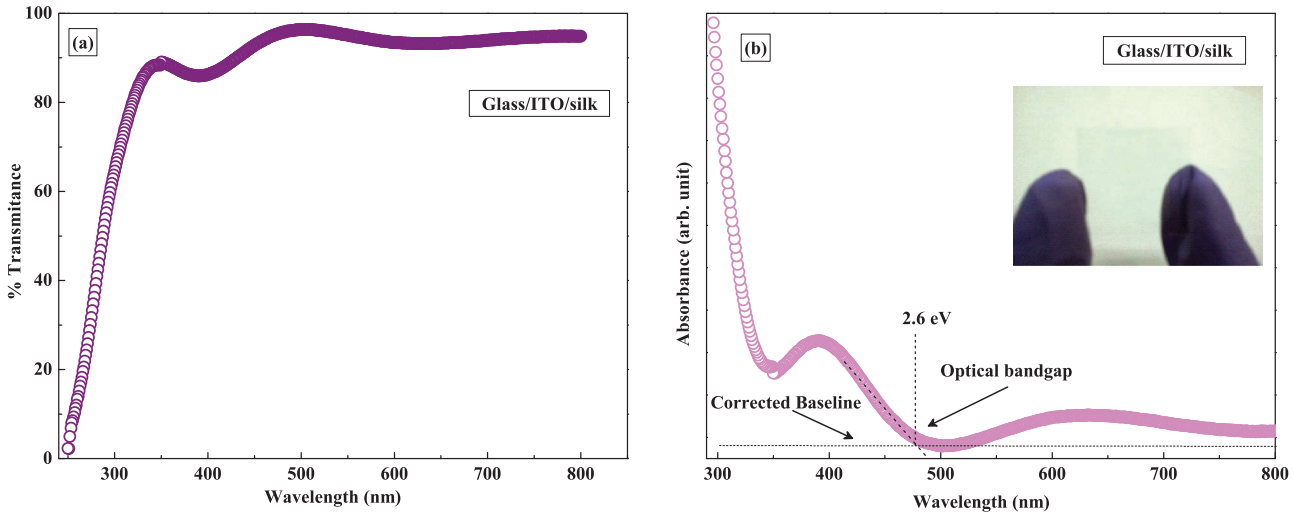

Figure 1. Optical characterization of silk fibroin protein films. a) Experimentally measured transmission spectrum of silk fibroin thin film spin coated on ITO/glass. b) Experimentally measured UV-vis absorption spectrum of silk fibroin thin film for optical bandgap determination. Photograph of the spin coated silk fibroin thin film on ITO coated glass (inset).

fibroin primarily consists of glycine, alanine, and serine in the molar ratio of 3:2:1, which forms typical -(-Ala-Gly-)$_n$- repeating sequences.[32] In order to estimate optical band gap of silk, values of UV-vis absorption spectra were measured (Figure 1b). The corresponding wavelength to the band gap energy can be calculated from the cross point of absorption onset line and corrected base line.[33] This was found to be around 476 nm and the optical band gap was estimated to be around 2.6 eV.

The idea of the memristor is to have two distinct memristive states that can be written at a specific voltage and non-destructively read with another voltage. Indeed, memristive switching in memristors exhibits large hysteresis (pinched hysteretic loops) in its current-voltage (I–V) characteristics.[2] Therefore, the devices could reversibly be switched between high resistance state (HRS) and low resistance state (LRS) in dc sweep or pulse mode. **Figure 2**a demonstrates the memristive switching of silk fibroin memristor by showing typical pinch hysteresis-like current-voltage characteristics on a linear scale obtained by sweeping the dc bias in 4 steps (0→+14 → 0→−14 → 0) without any electroforming process. Indeed, bipolar memristive switching characteristics are observed. Initially, the device remains in its high resistance state, *i.e.* in 'OFF' state at a smaller bias. When the applied bias reaches a threshold, resistance of the device increases abruptly resulting in a sudden increase in the current value, hence the device reaches on its SET condition, i.e., ON state (here it is at ≈ +10.4 V). Nevertheless, the reset process, i.e., switching from LRS to HRS, happens at negative voltage (≈ −11.5 V). To confirm the memristive phenomenon in the devices, the I-V characteristics are fitted with the model proposed by Yang *et al.*,[3] which consists of an equivalent circuit, and includes a rectifier in parallel with a memristor (inset of Figure 2a). The observed rectifying nature in I–V characteristics as shown in Figure 2a suggests that silk can make a rectifier contact with either electrode. The experimental data shows an excellent fit with the relation given below:[3]

$$I = \omega^m \xi \sinh(\eta V) + \zeta\left[\exp(\lambda V) - 1\right] \quad (1)$$

The first term in Equation 1 represents the electron tunneling through a thin residual barrier for the SET region of the memristor. Other important parameter ω, which represents the state variable of the memristor, is defined as the time integral of the voltage applied to the device. The SET or RESET state depends on this parameter. The state variable is a physical quantity that can be derived from the microscopic properties of the system. It is an explicitly dynamic in nature, i.e., the present state is dictated by biasing history.[2] Hence, it also signifies the non-volatile nature of the device. The direct proportional relationship between the drift velocity of the electrons and the applied bias could be characterized with the unity value of m. The other two parameters ξ and η are the fitting parameters. The second term of the above equation represents the rectifier effect to the memristor. The RESET portion of the I–V characteristics can be modulated by the two fitting parameters ζ and λ. The fitting parameters are listed in **Table 1**. It is noteworthy that the higher value of m greater than unity signifies the highly nonlinear dependence of the effective vacancy drift velocity upon applied voltage to the device.[2] As shown in Figure 2a, metal-insulator-metal (MIM) capacitors with the silk fibroin protein shows the memory resistor and rectifying characteristics at the same time, i.e., they are memristive in nature. Moreover, in order to evaluate the potentiality of silk fibroin protein for application in memristor devices, the endurance and retention characteristics have been examined. During endurance measurement READ voltage (V_{read}), which is chosen at a lower voltage than the threshold voltage of the device is often applied in order to READ the state of the device. Hence, in the present experiment the READ voltage has been at 4 V, and corresponding endurance characteristics for one bit operation have been performed, which is shown in Figure 2b. The corresponding SET and RESET pulses have alternately been triggered to make the device in its ON and OFF states,

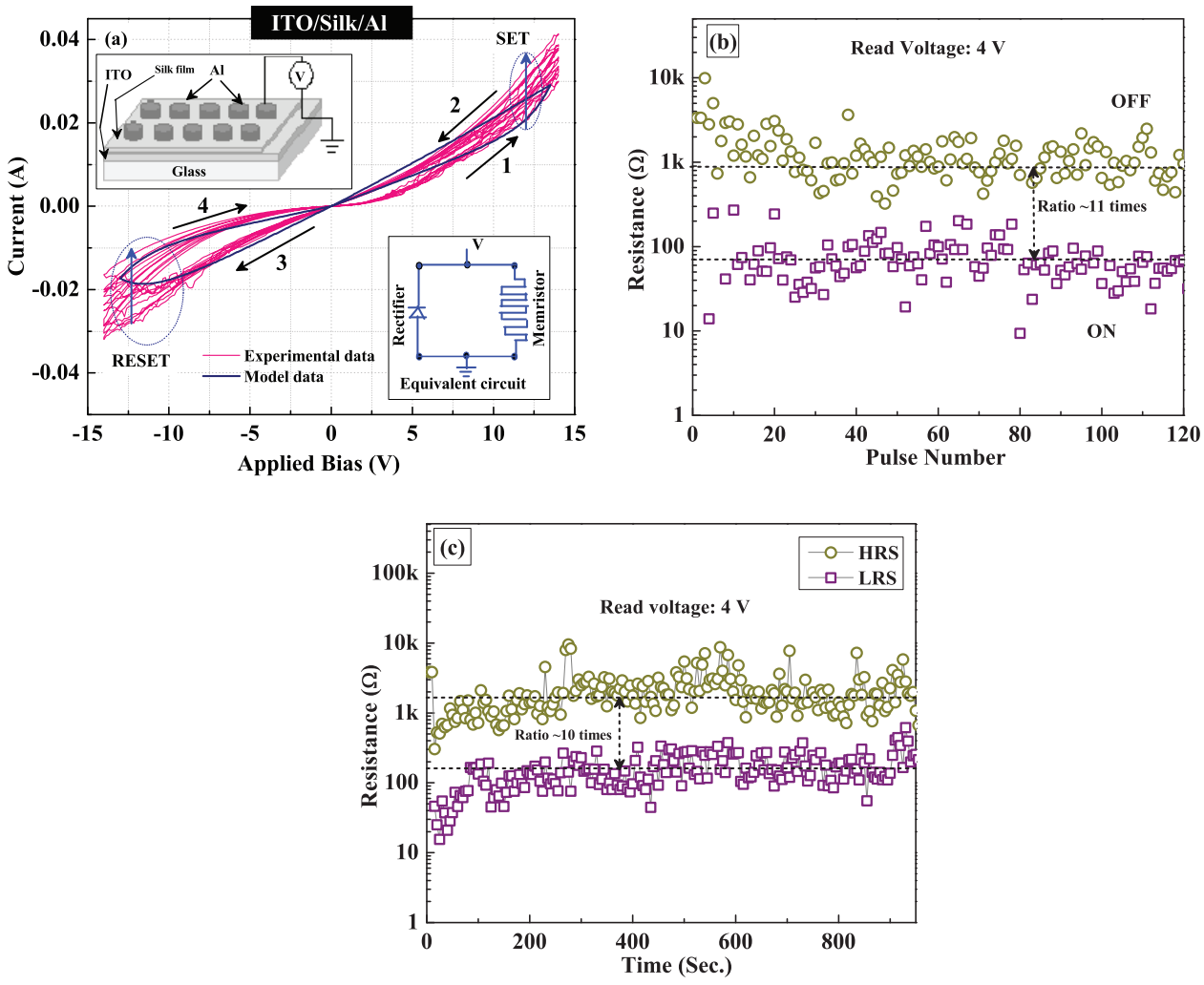

Figure 2. Bipolar reversible and nonvolatile switching characteristics of transparent bio-memristor devices with silk fibroin protein. a) Experimental (solid) and modeled (dotted) *I–V* characteristics of silk memristor. *I–V* characteristics in the SET condition exhibit a symmetric sinh-like curve, while that of RESET condition shows an asymmetric rectifying curve. The corresponding schematic of fabricated memristor device is shown in upper inset. The equivalent circuit model consists of a rectifier in parallel with a memristor is shown in lower inset. b) Endurance and c) retention test of HRS and LRS of the ITO/silk/Al capacitor structures under a positive bias operation. The resistances were read at 4 V.

respectively. Figure 2c demonstrates the retention characteristics of the memristor device. A reasonable endurance and retention characteristics having an average of ≈10 to 11 times switching ratio are obtained that further ensure the potentiality of silk-based memristor devices. However, the observed endurance and retention are low compared to other reported devices based on transitional metal oxide based memristors.

Table 1. Parameters used for fitting the memristive *I–V* characteristics.

Sweep direction	ω	m	ξ	η	ζ	λ
0 to + V	0.5	33	−0.9	0.52	0.22	0.0092
+V to 0	0.48	22	−2.4	−0.86	0.125	0.011
0 to −V	0.42	17	30	−0.544	−0.68	−0.0027
−V to 0	0.49	21	19	0.583	0.56	0.0016

The reasons could be as follows: a) the switching mechanism depends on the type of resistive switching material, electrode material, bias amplitude/duration and even environmental conditions. In case of, transition metal oxide based materials e.g., TiO_2, HfO_2, Nb_2O_5 etc. change in the valence state of cations due to an oxygen migration or redox process results in a change in the electronic conductivity. In fact, the formation or rapture of the conducting spots are believed to be related to oxygen vacancies (either electrically neutral, V_0 or positively charged, V_0^{2+}) in the bulk of the insulator, which plays an important role in the memristive switching. Likewise, the switching mechanism in silk is different in many ways since no such inorganic metal ions or oxygen vacancies are involved and are described later in this paper. b) The other reason could be the device structure itself. It has been shown that the endurance and retention properties of a memristor can be improved significantly by considering several schemes; in the device design

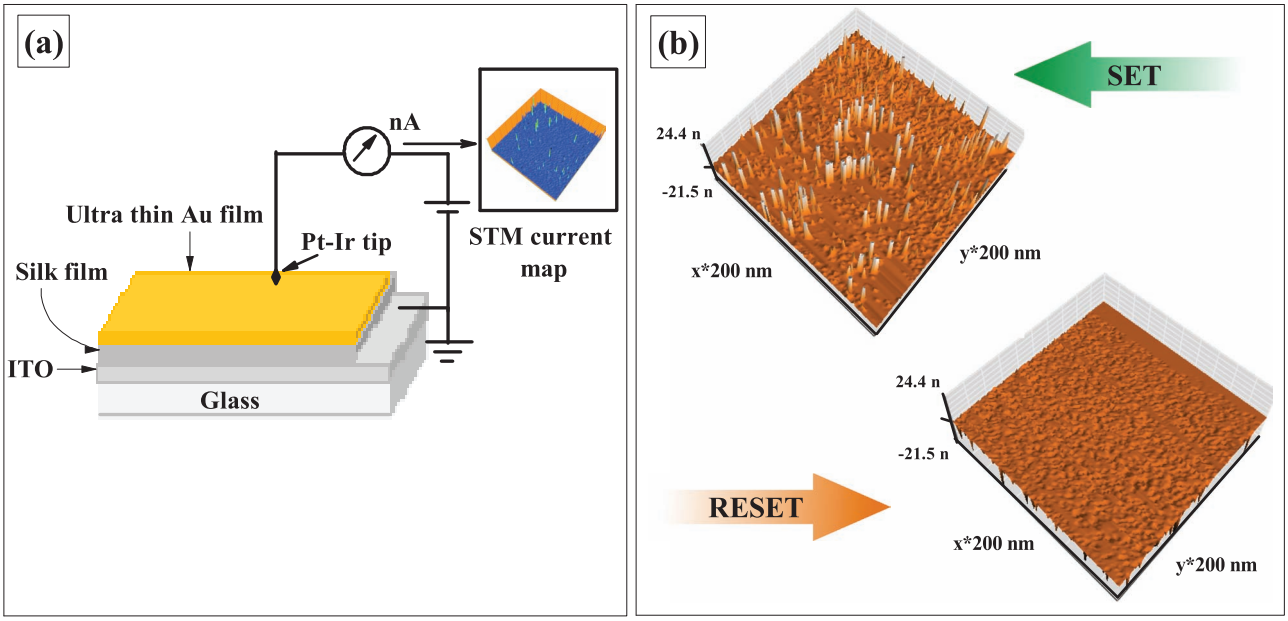

Figure 3. Local conductivity probing at nanoscale with scanning tunneling microscopy (STM). a) Simplified schematic diagram of the experimental setup. The local current imaging tunneling spectrum (CITS) can be obtained at each pixel during constant height imaging by applying a bias through the Pt-Ir tip. b) Nanoscale conductivity mapping of silk fibroin memristor devices during SET and RESET condition. The STM image shows a higher density of conducting spots or conducting filaments formation during SET condition while those disappear during RESET condition.

such as, 3- dimensional nano rod arrays or crossbar arrays compared to those simple planer (2D) device structures (the present device).[2,3] Similar endurance and retention characteristics with planer device architecture as observed in the silk memristors have also been observed in HfO_2-based memristors as has recently been reported by Yang et al.[34]

Furthermore, in order to probe switching mechanism in silk film at nanoscale, we used scanning tunneling microscopy (STM). Like other scanning probe microscope techniques, STM is also useful owing to its ability to reveal local surface information such as diverse topography, local electrical conduction (resistance), and surface potential variation (space charge distribution) in extremely high lateral resolution. Local electrical characteristics of the different features were obtained via the current imaging tunneling spectrum (CITS) technique. **Figure 3**a shows a simplified schematic diagram of the STM setup used in this study. A thin Au (5 nm) layer was used for better conduction with the STM tip. The thickness of Au layer is crucial here since we believe that with the use of such a thin metal (Au) layer, there will be no impact on the localized switching property of the silk film. With an applied bias through a Pt-Ir tip, local tunneling spectrum was obtained at each pixel during constant height imaging, i.e., the feedback circuit was temporarily disabled at each pixel and the current-voltage measurements were carried out. This phenomenon is also known as the localized conduction behavior of the dielectric film.[34,35] The bias was applied on the top ultrathin Au coated silk film (for stable electrical contact between the Pt-Ir tip and film surface) while the bottom electrode was kept at ground potential. The STM image shown in Figure 3b clearly represents local conducting spots (spikes in the current profile) over the scan area of 200 × 200 nm^2 after switching the sample to its SET condition. Meanwhile, in order to determine the RESET condition, the samples were scanned with a negative tip voltage as shown in Figure3b, which displays disappearance of almost all local conducting spots, suggesting the onset of RESET condition that enables the device to return to its HRS, as is also evident from the observed *I–V* characteristics (Figure 2a). Hence, the switching cycle resembles a typical nonvolatile memristor composed of ON and OFF states.

The basic structure of the silk fibroin is shown in **Figure 4**a. Basically, silk fibroin consists of two components, a light chain (≈25 kDa) and a heavy chain (≈390 kDa) present in a 1:1 ratio linked by a single disulphide bond.[35,36] Besides, in silk fiber, fibroin chains are aligned along the fiber axis held together by a close network of interchain hydrogen bonds with adjacent -(-Ala-Gly-)$_n$- sequences forming β-sheets structures. Details of the amino acid sequences of silk are described elsewhere.[37–40] Figure 4b shows the infrared absorption spectra of static amide I region of silk fibroin film. The broad feature observed in the spectrum is composed of a variety of components arising from the secondary structures in SF film. With the aim of gaining a better insight into its structural information, Fourier deconvolution procedure was performed. The bands between 1622 and 1627 cm^{-1} were assigned to β-sheets structures whereas those between 1660 and 1690 cm^{-1} to turn structures. In fact, the deconvoluted FTIR spectrum clearly represents all the constituents of SF film, which abbreviated as turns (T), alpha-helix (A), random coil (R), beta-sheets (B), and side chains (SC). Therefore, the silk film used in this work is amorphous and FTIR-ATR spectrum further confirms.

To study the physico-chemical origin of memristive switching properties of silk, electrochemical analyses were carried out using cyclic voltammetry technique; the cyclic voltammogram

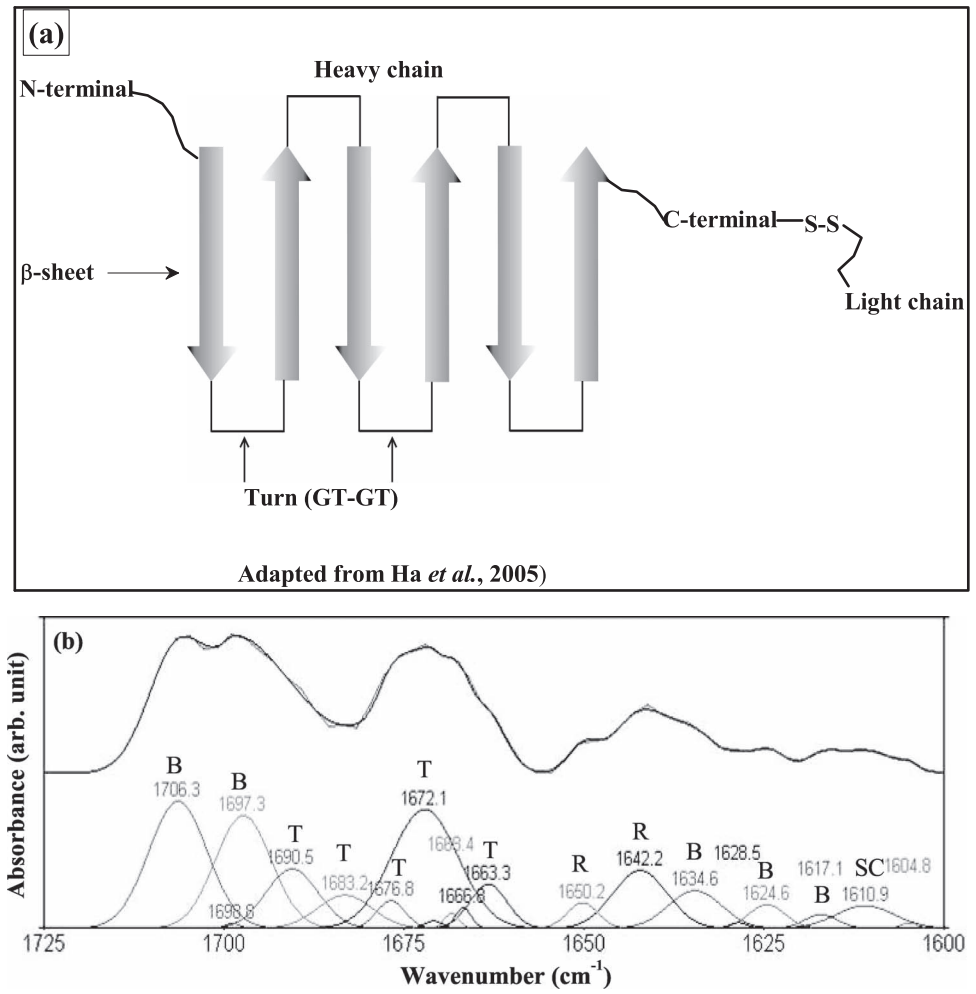

Figure 4. Structural analysis of silk fibroin. a) 2D schematic of the silk fibroin heavy chain and light chain.[34,35] b) FTIR-ATR spectrum of silk fibroin thin film deposited on ITO/glass. The silk fibroin consists of turn (T), random coil (R), β-sheet, and side chain; according to the curve-fitting results.

of silk is shown in **Figure 5**a. The onset potential for oxidation of the silk fibroin film was estimated to be around 0.33 V, as observed from the cyclic voltammogram, which corresponds to the removal of an electron from the HOMO (highest occupied molecular orbital) energy levels. Based on this study here we proposed the energy band diagram with HOMO/LUMO levels

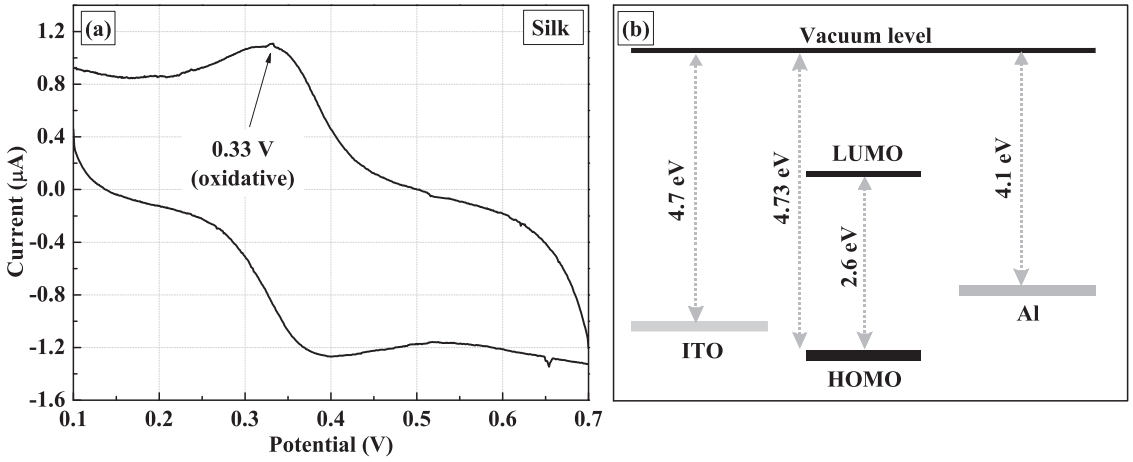

Figure 5. Electrochemical analysis of silk fibroin protein film. a) Cyclic voltammograms of silk fibroin thin film and b) proposed energy band diagram of Al/silk/ITO memristor device.

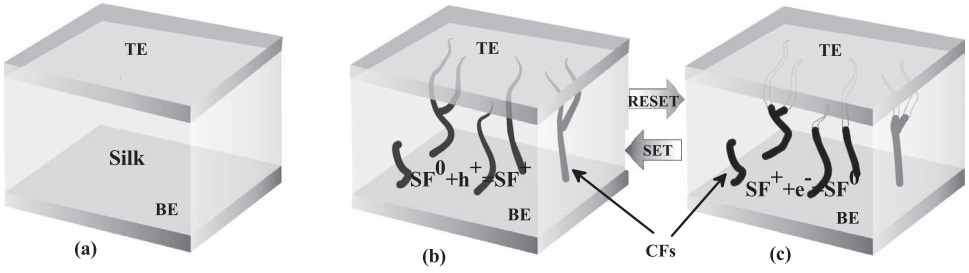

Figure 6. Proposed physical model to explain the switching mechanism of silk fibroin memristors. a) Virgin device condition, i.e., before applying any forming bias. b) Forming/SET condition is achieved with positive bias. During SET condition local oxidation (SF^+) takes place and a soft breakdown event occurs when the density of SF^+ reaches a critical value such that a percolation path is formed. c) RESET condition is achieved with negative bias. The device returns to its fresh-like HRS due to rupture of conductive SF^+ chains.

of silk fibroin, in addition to ITO and Al work functions as shown in Figure 5b. The two metal electrodes in combination with silk film were found to be good candidates as potential active layer for bio-memristor cells in terms of materials for bio-memristors, especially those based on energy concepts.

Founded upon the above experimental observations, a physical model is proposed. **Figure 6** illustrates different states of the memristive switching phenomenon. Initially, the device is in off-state, i.e., in high resistance state as shown in Figure 6a. Indeed the switching characteristics in silk fibroin (SF) are attributed to the formation and rupture of conducting filaments (CFs), which correspond to oxidation and reduction of the SF film as has been confirmed by the cyclic voltametric measurements. The oxidation state of SF (SF^+) is the low resistance state while the reduction state (SF^0) is the high resistance state. When a positive voltage is applied during the set process, the holes are injected from LUMO into the film; consequently SF^0 is oxidized into SF^+ ($SF^0+h^+ = SF^+$). In such a case, SF^0 serves as a charge-trapping site. However, during gradual increases in positive voltages, charge trapping in SF^0 leads to the accumulation of space charges. Hence, if there are sufficient numbers of SF^+ chains and CFs are formed, as a result of which sudden increase in current values (It may occurs at higher voltage than the oxidation voltage, as can be seen from *I–V* data) are observed and subsequently the device reaches its ON-state, i.e., in the low resistance state (Figure 6b). On the other hand, when a negative voltage is applied during the reset process, the electrons are injected from the HOMO into the SF film, thus SF^+ is reduced into SF^0 ($SF^+ + e^- = SF^0$), which results in rupture of the conductive SF^+ filaments. Finally, the device again returns to its fresh-like high resistance state when sufficient CFs demolition takes place to "switch OFF"; the remaining percolation path as shown in Figure 6c.

3. Conclusions

In summary, transparent bio-memristor devices are fabricated with natural regenerated silk fibroin protein obtained from cocoons of *Bombyx mori* silkworm. The electronic-grade silk aqueous solution exhibits high transparency across most of the visible spectrum. Bipolar memristive switching behavior is demonstrated and the switching mechanism is confirmed to be due to the filamentary switching. Scanning tunneling microscopy is used to probe local conduction behavior at nanoscale. A physical model is also proposed to explain the experimental observations based on the carrier trapping and/or detrapping in silk films due to oxidation and reduction procedures as evidenced from cyclic voltammetry measurements. Indeed, the back and forth transition between oxidation and reduction state of silk subjected to different applied electric field or electroforming process plays an important role in memristive switching. The interesting memristive properties as observed in silk protein may find application as a memristor in advanced bio-inspired very large scale integrated circuit design. This may prove to be useful in making the hybrid complementary metal oxide semiconductor devices, neuron/memristor-synapse approach.

4. Experimental Section

Silk fibroin solution was prepared using *Bombyx mori* cocoons following a standard protocol.[27–29] Briefly, the silkworm cocoon cut pieces were boiled in 0.02 M aqueous solution of Na_2CO_3 for 30 mins for degumming, i.e., the removal of glue like silk protein sericin.[30,31] The silk fibers were then washed and solubilized in 9.3 M lithium bromide (LiBr) solution at 50 °C. The resultant solution was dialyzed against deionized water for removal of traces of LiBr followed by centrifugation at 9000 rpm for 10 min to yield silk fibroin protein solution (2 wt%).

An ITO-coated glass (Corning-9000) substrate to be used was cleaned sequentially with water, acetone and 2-propanol in an ultrasonic bath for 10 min. The silk fibroin aqueous solution was then spin-coated onto the optically transparent ITO coated glass substrates at room temperature. A 60 nm thick ITO layer acted as the bottom contact. Physical thickness of the silk film, as measured with a surface profilometer (Veeco Decktak 150), was found to be around 400 nm. Finally, a thick Al top electrode was thermally evaporated at a pressure of $\approx 10^{-6}$ Torr through a shadow mask having an area of 1.96×10^{-3} cm^2. The optical transmittance measurements were performed with a Varian Cary 5000 UV/vis spectrophotometer in the wavelength ranging from 300 to 800 nm, and its bonding structure was determined using Fourier transform infrared-attenuated total reflection (FTIR-ATR, Thermo Nicolet Nexus 870). The FTIR-ATR spectrum was acquired over the range of 4000–400 cm^{-1} with a spectral resolution of 2 cm^{-1}. The scanning tunneling microscopy (STM) measurements were performed using Nanosurf easyScan 2 instrument with a Pt-Ir tip, and electrochemical analyses were performed on a CHI 630a Electrochemical Workstation (CH Instruments, USA). All the electrochemical experiments were measured in a three-electrode system, in which a platinum wire was acted as a counter electrode and a saturated calomel electrode as reference electrode. A silk coated ITO electrode was used as working electrode. Cyclic voltammetry measurements were performed in 0.01 M hydrochloric acid solution

(pH 2.0) as supporting electrolyte. The electrical measurements were carried out using the Agilent 4156C semiconductor parameter analyzer at room temperature in conjunction with a fully automated computerized measurement system.

Acknowledgements

This work was financially supported by Department of Science and Technology (funding for MGS project), Department of Chemistry (Indian Institute of Technology, Kharagpur), Department of Biotechnology and its Bioinformatics facility (SCK), Council of Scientific and Industrial Research (fellowship to BK), Government of India, New Delhi.

Received: January 10, 2012
Revised: May 28, 2012
Published online: July 3, 2012

[1] L. O. Chua, *IEEE Trans. Circuit Theory* **1971**, *18*, 507.
[2] D. B. Strukov, G. S. Snider, D. R. Stewart, R. S. Williaws, *Nature* **2008**, *453*, 80.
[3] J. J. Yang, M. D. Pickett, X. Li, D. A. Ohlberg, D. R. Stewart, R. S. Williams, *Nat. Nanotechnol.* **2008**, *3*, 429.
[4] L. O. Chua, *Appl. Phys. A* **2011**, *102*, 765.
[5] V. Erokhin, T. Berzina, A. Smerieri, P. Camorani, S. Erokhina, M. P. Fontanaa, *Nano Commun. Networks* **2010**, *1*, 108.
[6] C. Kügeler, R. Rosezin, E. Linn, R. Bruchhaus, R. Waser, *Appl. Phys. A* **2011**, *102*, 791.
[7] R. Waser, M. Aono, *Nat. Mater.* **2007**, *6*, 833.
[8] K. Szot, M. Rogala, W. Speier, Z. Klusek, A. Besmehn, R. Waser, *Nanotechnology* **2011**, *22*, 205601.
[9] G. Liu, X. Zhuang, Y. Chen, B. Zhang, J. Zhu, C. X. Zhu, K. G. Neoh, E. T. Kang, *Appl. Phys. Lett.* **2009**, *95*, 253301.
[10] Z. S. Wang, F. Zeng, J. Yang, C. Chen, Y. C. Yang, F. Pan, *Appl. Phys. Lett.* **2010**, *97*, 253301.
[11] P. Y. Lai, J. S. Chen, *Org. Electron.* **2009**, *10*, 1590.
[12] P. Y. Lai, J. S. Chen, *Appl. Phys. Lett.* **2008**, *93*, 153305.
[13] F. Meng, L. Jiang, K. Zheng, C. F. Goh, S. Lim, H. H. Hng, J. Ma, F. Boey, X. Chen, *Small* **2011**, *7*, 3016.
[14] M. Singh, H. M. Haverinen, P. Dhagat, G. E. Jabbour, *Adv. Mater.* **2010**, *22*, 673.
[15] S. Talukdar, M. Mandal, D. W. Hutmacher, P. Russell, C. Soekmadji, S. C. Kundu, *Biomaterials* **2011**, *32*, 2149.
[16] S. Talukdar, Q. T. Nguyen, A. C. Chen, R. Sah, S. C. Kundu, *Biomaterials* **2011**, *8*, 027.
[17] N. Bhardwaj, Q. T. Nguyen, A. C. Chen, R. T. Sah, S. C. Kundu, *Biomaterials* **2011**, *32*, 5773.
[18] B. Kundu, S. C. Kundu, *Prog. Polym. Sci.* **2010**, *35*, 1116.
[19] R. Capelli, J. J. Amsden, G. Generali, S. Toffanin, V. Benfenati, M. Muccini, D. Kaplan, F. G. Omenetto, R. Zamboni, *Org. Electron.* **2011**, *12*, 1146.
[20] C. H. Wang, C. Y. Hsieh, J. C. Hwang, *Adv. Mater.* **2011**, *23*, 1630.
[21] D. H. Kim, Y. S. Kim, J. Amsden, B. Panilaitis, D. L. Kaplan, F. G. Omenetto, M. R. Zakin, J. A. Rogers, *Appl. Phys. Lett.* **2009**, *95*, 133701.
[22] H. Tao, J. J. Amsden, A. C. Strikwerda, K. Fan, D. L. Kaplan, X. Zhang, R. D. Averitt, F. G. Omenetto, *Adv. Mater.* **2010**, *22*, 3527.
[23] B. D. Lawrence, M. C. Golomb, I. Georgakoudi, D. L. Kaplan, F. G. Omenetto, *Biomacromolecules.* **2008**, *9*, 1214.
[24] C. J. Bettinger, K. M. Cyr, A. Matsumoto, R. Langer, J. T. Borenstein, D. L. Kaplan, *Adv. Mater.* **2007**, *19*, 2847.
[25] A. B. Mathur, V. Gupta, *Nanomedicine* **2010**, *5*, 807.
[26] F. G. Omenetto, D. L. Kaplan, *Nat. Photonics* **2008**, *2*, 641.
[27] S. Sofia, M. B. McCarthy, G. Gronowicz, D. L. Kaplan, *J. Biomed. Mater. Res.* **2001**, *54*, 139.
[28] S. T. Parker, P. Domachuk, J. Amsden, J. Bressner, J. A. Lewis, D. L. Kaplan, F. G. Omenetto, *Adv. Mater.* **2009**, *21*, 2411.
[29] S. C. Kundu, B. C. Dash, R. Dash, D. L. Kaplan, *Prog. Polym. Sci.* **2008**, *33*, 998.
[30] C. Acharya, B. Hinz, S. C. Kundu, *Biomaterials* **2008**, *29*, 4665.
[31] J. Kundu, M. Dewan, S. Ghoshal, S. C. Kundu, *J. Mater. Sci. Mater. Med.* **2008**, *19*, 2679.
[32] R. E. Marsh, R. B. Corey, L. Pauling, *Biochim. Biophys. Acta* **1955**, *16*, 1.
[33] R. Schlaf, P. G. Schroeder, M. W. Nelson, B. A. Parkinson, C. D. Merritt, L. A. Crisafulli, H. Murata, Z. H. Kafafi, *Surf. Sci.* **2000**, *450*, 142.
[34] J. J. Yang, M.-X. Zhang, J. P. Strachan, F. Miao, M. D. Pickett, R. D. Kelley, G. M. Ribeiro, R. S. Williams, *Appl. Phys. Lett.* **2010** *97*, 232102.
[35] Y. C. Ong, D. S. Ang, K. L. Pey, S. J. O'Shea, K. E. Goh, C. Troadec, C. H. Tung, T. Kawanago, K. Kakushima, H. Iwai, *Appl. Phy. Lett.* **2007**, *91*, 102905.
[36] D. H. Kwon, K. M. Kim, J. H. Jang, J. M. Jeon, M. H. Lee, G. H. Kim, X. S. Li, G. S. Park, B. Lee, S. Han, M. Kim, C. S. Hwang, *Nat. Nanotechnol.* **2010**, *5*, 148.
[37] M. Krejchi, S. Cooper, Y. Dequchi, E. Atkins, M. Fournier, T. Mason, D. Tirrell, *Macromolecules* **1997**, *30*, 5012.
[38] S. W. Ha, H. S. Gracz, A. E. Tonelli, S. M. Hudson, *Biomacromolecules* **2005**, *6*, 2563.
[39] R. E. Marsh, R. B. Corey, L. Pauling, *Biochim. Biophys. Acta.* **1955**, *16*, 1.
[40] S. Inoue, K. Tanaka, F. Arisaka, S. Kimura, K. Ohtomo, S. Mizuno, *J. Biol. Chem.* **2000**, *275*, 40517.